NUMERICAL STUDY OF THE EFFECT OF THE OPPOSING JET ON REDUCTION OF AERODYNAMIC HEATING WITH DIFFERENT NOSE CONFIGURATIONS

Isao Tamada, Shigeru Aso and Yasuhiro Tani
Space Transportation Systems Lab., Department of Aeronautics and Astronautics, Kyushu University, Fukuoka, Japan

Keywords: *Opposing jet, thermal protection system, reusable launch vehicle, turbulent flow*

Abstract

The opposing jet is proposed for aerodynamic heat reduction. In this study, the opposing jet has been applied for three nose configurations, including ogive body, blunt body and ogive body with extended nozzle, to investigate the efficient nose configuration for the opposing jet.

Numerical study has been implemented for the supersonic flow at $M_\infty = 3.98$ and the results showed that there is a direct correlation between the applied nose configuration and the effect of the opposing jet. Detail flow field analysis revealed that to avoid constructing the strong recompressed shock is important and essential to reduce the aerodynamic heating by using the opposing jet.

Of all three nose configurations, it was found that the ogive body with extended nozzle is the most effective model as for reduction of aerodynamic heat because significant heat flux reduction was acquired with smaller mass flow rate jet compared to other nose configuration.

Nomenclature

PR	Total pressure ratio $p_{0j}/p_{0\infty}$
$P_{0\infty}$	Freestream total pressure [MPa]
P_{0j}	Jet total pressure [MPa]
M_∞	Freestream Mach number
M_j	Jet Mach number
q_w	Heat flux into the wall [W/m^2]
d_j	Jet orifice diameter [mm]
$T_{0\infty}$	Freestream total temperature [K]
T_{0j}	Jet total temperature [K]
T_w	Wall temperature [K]
s	Distance from the nose tip along the wall [mm]
Re	Reynolds number based on model diameter
D	Drag force [N]
D_p	Form drag [N]
D_f	Frictional drag [N]
D_j	Drag force by the opposing jet [N]
C_D	Drag coefficient

1 Introduction

In the design of reusable launch vehicle (RLV), aerodynamic heating is one of the most important problems to be solved because very high heat due to the strong shock wave damages the RLV body at the reentry stage. Therefore, it is necessary to develop a suitable thermal protection system for similar challenging circumstances.

Thermal protection systems are classified into two categories; passive methods and active methods. Among the active methods, the opposing jet has been proposed by the previous studies [1], [2], [3], [4], and proved to be effective by those works. Fig.1 shows the general flow field of this thermal protection system. Flow field will change depending on the total pressure ratio PR. Aerodynamic heat reduction could be obtained by what cold recirculation region and jet stream cover the nose region.

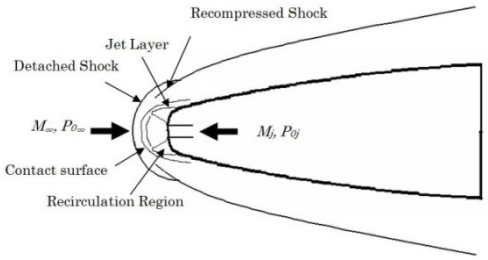

Fig.1. General flow field of the opposing jet in supersonic freestream

Since this system has high reusability, it is suitable for RLV. However, the previous study was conducted only for the blunt body. In practice, the shaper shape like an ogive body is usually adopted for the nose shape to reduce the drag rather than the blunt shape.

The objective of the present study is to investigate whether the opposing jet is effective for the ogive body, and to find out the more effective nose configuration other than the blunt body for applying the opposing jet.

2 Numerical Methodology

2.1 Governing Equation and Turbulence Model

In this work, two-dimensional Axisymmetric Reynolds-Averaged Navier-Stokes equations are used as the governing equation. Inviscid term is calculated by AUSM-DV scheme [5] with MUSCL interpolation to keep spatially second-order. The Viscous term is computed by spatially second-order central difference method. Full LU-ADI factorization algorithm [11] is adopted for time integration.

The Turbulence model is essentially required to calculate this complex flow field. Then, the Wilcox (1998) $k-\omega$ model is chosen as the turbulence model. By the previous work [6], this model is proved to be superior in numerical stability to $k-\epsilon$ model and the other $k-\omega$ models mainly in the viscous sublayer near the wall and can predict the flow separation better in terms of its size and physical properties. Since precise prediction for the size of recirculation region and physical properties near the wall are required in this study, this model is considered to be suitable. However, this model has a couple of numerical problems; numerical sensitivity to small freestream value of ω in free-shear region [6] and excessive production of turbulent energy behind the strong shock and at the region where two different flows collide [7].

To avoid the latter problem, turbulent viscosity has been modified by the coefficient C_μ proposed by Craft et.al [8]. The coefficient C_μ is basically used in $k-\epsilon$ model for the same purpose, but because there is a correlation between the dissipation rate per unit mass ϵ and the specific dissipation rate ω, this coefficient can be used in Wilcox (1998) $k-\omega$ model. Therefore, new turbulent viscosity is calculated by the following equation. β^* is the closure coefficient for $k-\omega$ model.

$$\mu_t = \frac{C_\mu}{\beta^*}\frac{\rho k}{\omega} \qquad (1)$$

The former problem related to the freestream condition will be discussed in the section 3.1.

2.2 Model and Numerical Grid

In this paper, the flow fields of the both blunt and ogive body have been simulated to compare the effect of the opposing jet on aerodynamic heating and the drag between the two nose configurations. To improve the effect of the opposing jet, the ogive body with extended nozzle configuration is also considered.

Although the wind tunnel experiment for the ogive body without opposing jet has been implemented as stated below, the experiment with opposing jet has not been conducted yet. Therefore, the models used in this study have been set as the experimental models for predicting the effect of the opposing jet. Those models are the blunt body and the von-Karman ogive body with rounded nose which radius is 7.5 mm. The diameters of the models are 40 mm and each body has the same volume. The jet orifice diameter has been set as 2 mm for both configurations. Prior to this experiment, the experiment for the ogive configuration without opposing jet was conducted in the supersonic wind tunnel at JAXA/ISAS, Institute of Space and Astronautical Science in Japan. The data acquired by this wind tunnel test has been used for validating the code used in this study as stated in the next section.

The configurations of numerical grids for each shape are shown in Fig.2 and 3 respectively. Each grid has 350×150 points for the ogive body and 240×150 points for the blunt body. Moreover, since it can be expected that the flow field would likely be complicated around the jet orifice, the gird points were

clustered around this region. In fact, the jet orifice has 41 points within the radius of 1 mm.

The minimum grid spacing just next to the wall has been set as 1×10^{-3} mm to accurately predict the heat flux into the wall.

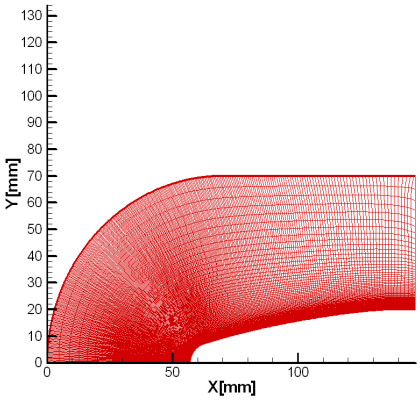

Fig.2. Grid for the ogive body

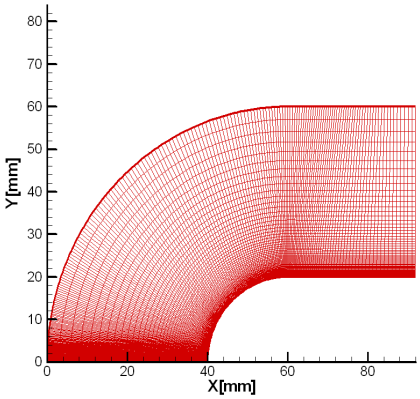

Fig.3. Grid for the blunt body

2.3 Validation of Numerical Code

Although the code used in this study has been validated by Hayashi [1], it is for only the blunt body. Thus, it is necessary to investigate if this code would be also valid for the different shape, i.e. the ogive body. Therefore, this code has been validated by using the wind tunnel data.

The wind tunnel test has been conducted with three different freestream conditions, which is listed in Table.1.

Table.1. Freestream conditions of experiment

M_∞	$P_{0\infty}$ [MPa]	$T_{0\infty}$[K]	T_w [K]	Re
1.30	0.15	300	300	1.16×10^7
2.00	0.21	300	300	1.33×10^7
4.00	0.50	300	300	1.16×10^7

Fig.4 shows gauge pressure distributions of the experimental and numerical results and the corresponding static pressure contour of $M_\infty = 1.3$ case. In this figure x represents the distance from the tip of nose along the axis. Numerical gauge pressure has been calculated just by subtracting atmospheric pressure from the static pressure acquired through the simulation. From this figure, it can be seen that numerical pressure distribution is fairly consistent with the experimental data. In addition to that, numerical result could capture the radical pressure drop around the tip of nose due to the expansion wave and sequential pressure rise due to the recompressed shock.

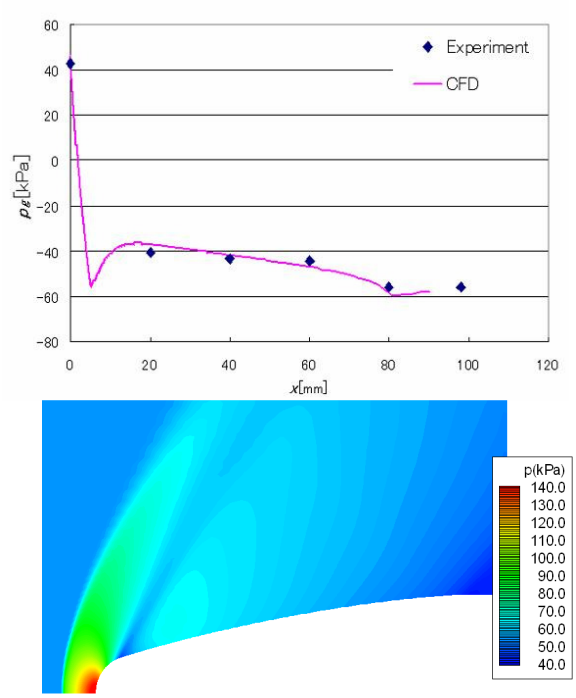

Fig.4. Gauge pressure distributions and static pressure contour of $M_\infty = 1.3$ case

To investigate the qualitative consistency, Schlieren photographs and x-direction density gradient were compared in Fig.5. In the x-direction density gradient pictures, the white region represents the positive density transition and black region expresses the negative one. According to this figure, numerical result has fair qualitative consistency with experimental data. Thus, this scheme has enough capability to simulate the supersonic flow and capture the shock wave at the precise location. Therefore, this numerical code has enough accuracy to

discuss the thermophysics of the flow field around ogive body with opposing jet.

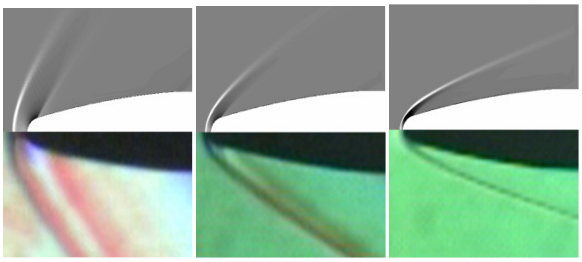

$M_\infty = 1.3$ $M_\infty = 2.0$ $M_\infty = 4.0$

Fig.5. Comparison of numerical density gradient (upper) and Schlieren photographs (lower)

3 Numerical Results and Discussion

3.1 Flow Conditions

Flow conditions have been set as listed in Table.2. The previous work [1] was referred to determine the freestream conditions. As stated in the introduction, because total pressure ratio PR is dominant parameter for the flow field configuration and the opposing jet effect on aerodynamic heat reduction, only this parameter is varied in each case.

Boundary condition on the wall is simply non-slip condition for velocity and turbulent kinetic energy k. However, specific dissipation rate ω should be carefully determined at freestream and wall boundaries because of the inherent sensitivity of $k-\omega$ model to freestream value of ω. In this work, the values of ω at these boundaries have been used recommended values in the past paper [6].

Table.2. Flow conditions

<Freestream>		
Mach number	M_∞	3.98
Total pressure	$P_{0\infty}$[MPa]	1.38
Total temperature	$T_{0\infty}$[K]	404
<Opposing Jet>		
Mach number	M_j	1.0
Total temperature	T_{0j}[K]	300
Jet orifice diameter	d_j[mm]	2.0
Total pressure ratio	PR	0,0.6, 1.0, 2.0, 3.2
<Wall Condition>		
Wall temperature	T_w[K]	290

3.2 Comparison of Heat Flux

Since this study is aimed to investigate to what extent the opposing jet has thermal protection effect on ogive body, it is useful to compare heat flux distributions between ogive and blunt bodies.

Heat flux distribution for each body is shown in Fig.6 and 7 respectively with the nose configuration of each body. Heat flux value at the stagnation point was also calculated by Fay & Riddell's equation [9].

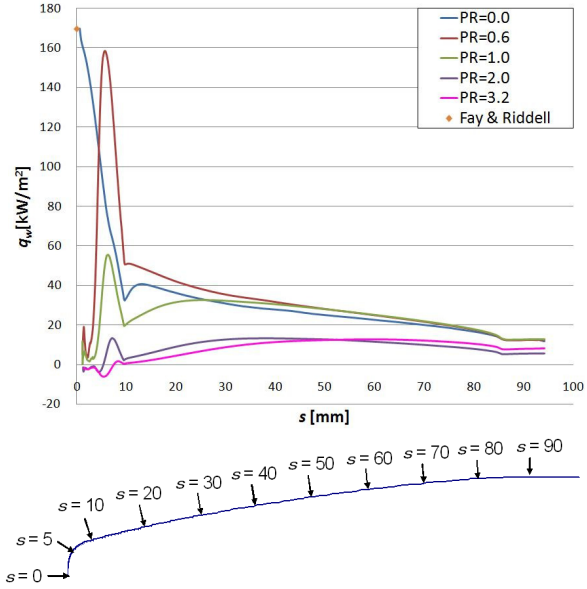

Fig.6. Heat flux distribution for ogive body

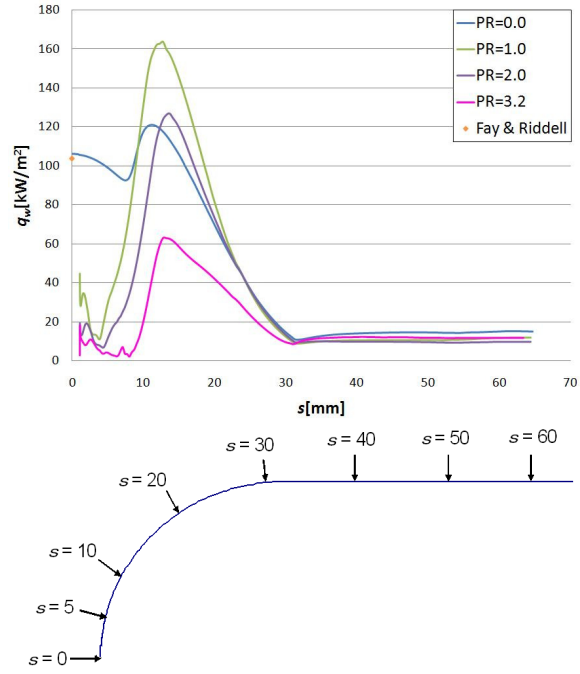

Fig.7. Heat flux distribution for blunt body

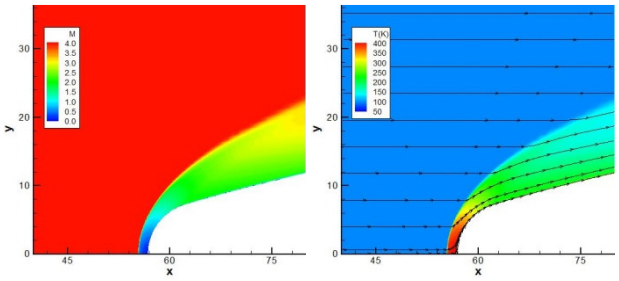

a) $PR = 0.0$

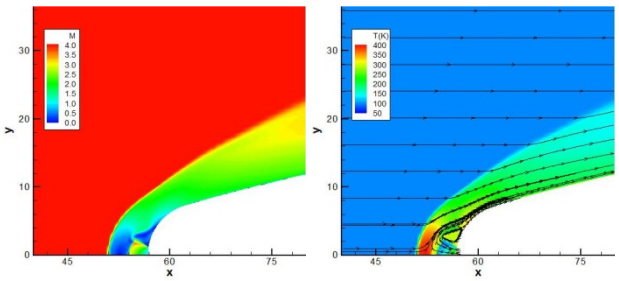

b) $PR = 0.6$

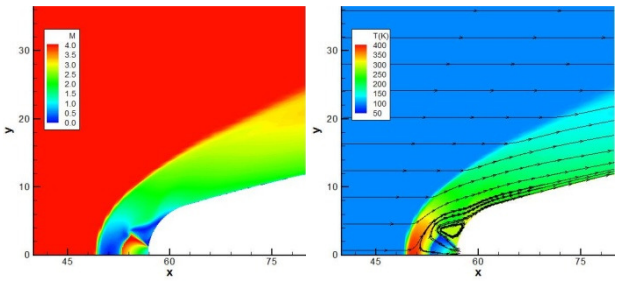

c) $PR = 1.0$

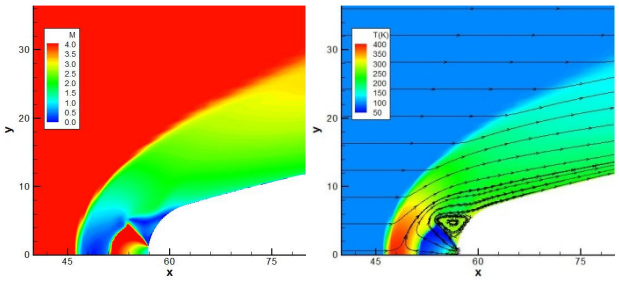

d) $PR = 2.0$

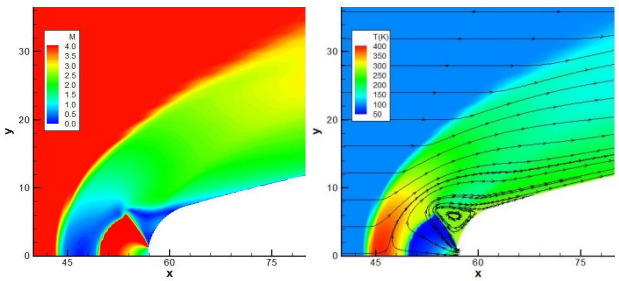

e) $PR = 3.2$

Fig.8. Mach contour (left) and temperature contour with streamline (right) for the ogive body

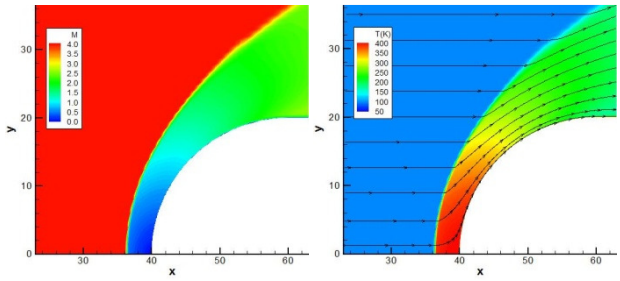

a) $PR = 0.0$

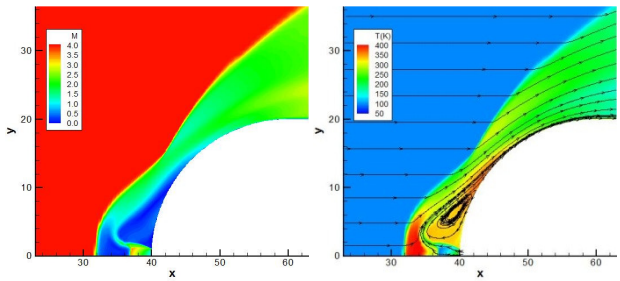

b) $PR = 0.6$ (Unstable)

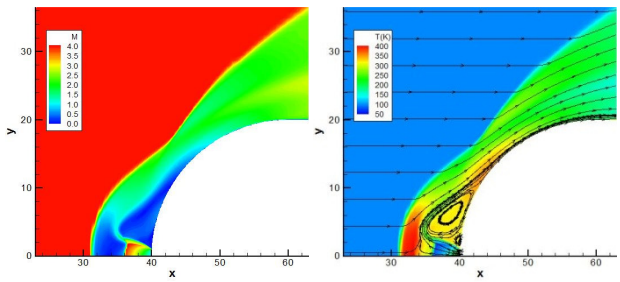

c) $PR = 1.0$

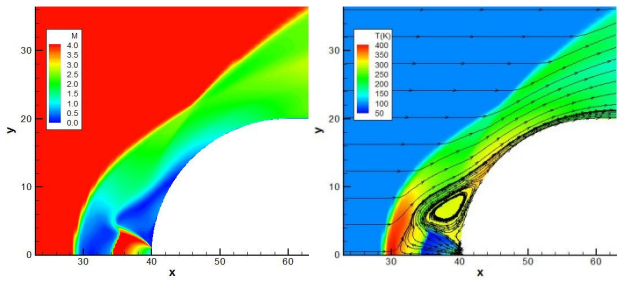

d) $PR = 2.0$

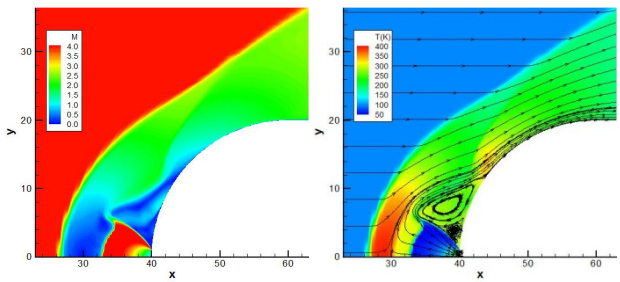

e) $PR = 3.2$

Fig.9. Mach contour (left) and temperature contour with streamline (right) for the blunt body

In the case of $PR = 0.6$ for the blunt body, unstable flow field was formed because self-induced oscillation occurred. Self-induced oscillation can result from small total pressure ratio as reported by Finley [10]. Since this study deals with only stable flow fields, that case has been excluded from the discussion, though the flow field is shown in Fig.9 b).

First of all, it can be mentioned that the opposing jet is effective to protect the ogive body from aerodynamic heating as well as in case of the blunt body. This thermal protection effect is gradually augmented as PR increases. Especially, the opposing jet succeeded to reduce heat flux over the entire ogive surface in the case of $PR = 3.2$ for the ogive body. The detail explanation for the mechanism of this thermal protection effect can be referred in [1].

However, as shown in Fig.6 and 7, in some cases maximum heat flux value which occurs around the reattached point ($s \approx 12$ mm) due to recompressed shock excesses heat flux in the case of no jet for both the ogive and blunt bodies. This undesired phenomenon occurs in the case of $PR = 0.6$ for the ogive body and $PR = 1.0, 2.0$ for the blunt body. All of these cases are stable flow field, i.e., no self-induced oscillation observed. According to Hayashi [1], if the flow field is self-induced oscillation, heat flux tends to excess that of the no jet case, which implies there should be unreported cause of this undesired phenomenon except for self-induced oscillation.

The difference of the ratio of jet orifice diameter to model diameter from the previous work is considered as a cause of this undesired phenomenon. In detail, that ratio is 0.05, while it was 0.08 in the past study. If this ratio becomes small under the same mass flow rate condition, the opposing jet is likely to be more under expanded as shown in Fig.10. As stated in the introduction, cold jet stream takes a main part on heat flux reduction. However, when the opposing jet gets more under expanded, less jet stream passes through the barrel shock. Then, less jet stream has less heat capacity due to smaller density and is heated by recompressed shock easily. Consequently, such undesired high heat flux could be observed around the reattach point. In Fig.7, although heat flux value gets also high at $s \approx 10$ mm even in no jet case for the blunt body, this is because of not the difference of the ratio of jet orifice diameter to model diameter, but turbulent transition around this point as reported in [1].

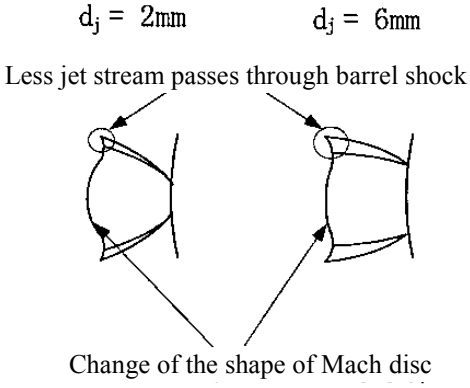

Fig.10. Under expansion of the opposing jet with different jet orifice diameter

This study also revealed that the opposing jet is much more effective for the ogive body than for the blunt body. Comparing Fig.6 from Fig.7 it can be seen that maximum heat flux around the nose tip due to recompressed shock is much lower in the ogive cases under the same total pressure ratio, or mass flow rate, condition. This result implies that the opposing jet has better thermal protection effect for ogive body rather than blunt one, because it can reduce more heat flux with smaller PR. The detail explanation for this result is followings.

Comparing between Fig.8 d) and Fig.9 d), although the recirculation region size itself is larger in the blunt case, there can be observed high temperature region right behind the recompressed shock. On the other hand, the recirculation region covers the entire nose in the ogive case, which leads freestream and jet stream to flow smoothly along the surface and, as a result, avoids constructing strong recompressed shock as it can be seen in the blunt case. That is why heat flux gets high behind recompressed shock in the blunt case, while it keeps low value even behind the recompressed shock in the ogive case. In other words, what is essential and important to reduce heat flux into the wall by ejecting the opposing jet is to avoid constructing strong recompressed shock.

3.3 Comparison of Drag and Drag Coefficient

The another main task of this study is to make sure that drag of the ogive body is smaller than that of the blunt body, and investigate how the opposing jet affects the drag force.

Drag force of both shapes in all cases are shown in Fig.11 and Fig.12 respectively. In calculating the drag force by the opposing jet, the equation below was used,

$$D_j = \dot{m}_j V_j + (p_j - p_{stag}) A_j \qquad (2)$$

where $\dot{m}_j$ is jet mass flow rate, V_j is jet velocity, p_j is jet static pressure, A_j is jet orifice area and p_{stag} is the stagnation point pressure in no jet case.

In these figures, form drag, frictional drag and drag force by the opposing jet and total drag are indicated. Comparing Fig.11 and 12, it can be seen that drag force of the ogive is much lower than that of the blunt in all cases. This low drag resulted from low form drag of the ogive body.

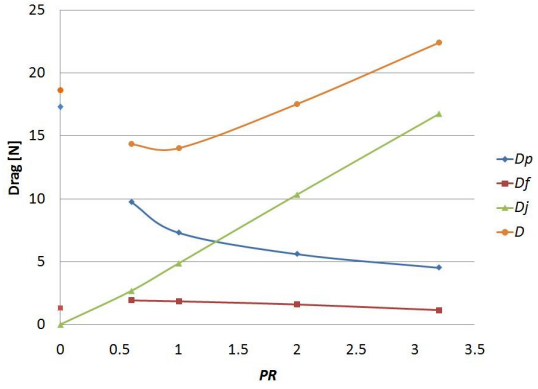

Fig.11 Each drag force of the ogive case

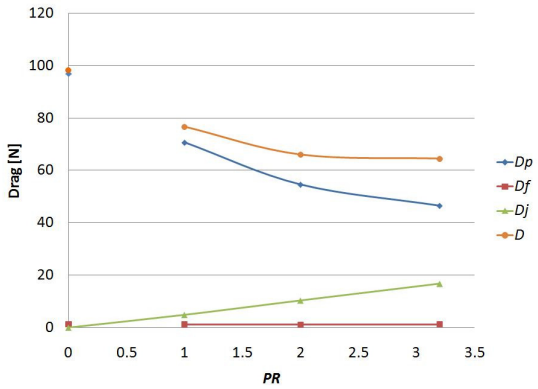

Fig.12 Each drag force of the blunt case

As PR increases, form drag decreases because low pressure recirculation region becomes larger and recompressed shock which mainly raises the form drag becomes weaker. On the other hand, drag force by the opposing jet becomes larger as PR increases. Although total drag starts to increase from $PR \approx 0.7$ for the ogive body because drag force by the opposing jet keeps increasing, it has been found that the ogive body shows lower drag forces than the blunt. As a reminder, the graph lines are not connected between $PR = 0.0$ and the next point because the self-oscillation can be predicted in those small PR regions as stated above.

Fig.13 shows drag coefficients of the ogive and blunt shapes. Drag coefficients are calculated with the usual equation, which is

$$C_D = \frac{D_{total}}{\frac{1}{2}\rho_\infty U_\infty^2 S} \qquad (3)$$

where S is the cross sectional area of the body. As mentioned above, since total drag of the ogive body is much lower than that of the blunt body, drag coefficient of the ogive body is also significantly lower than that of the blunt body for all cases.

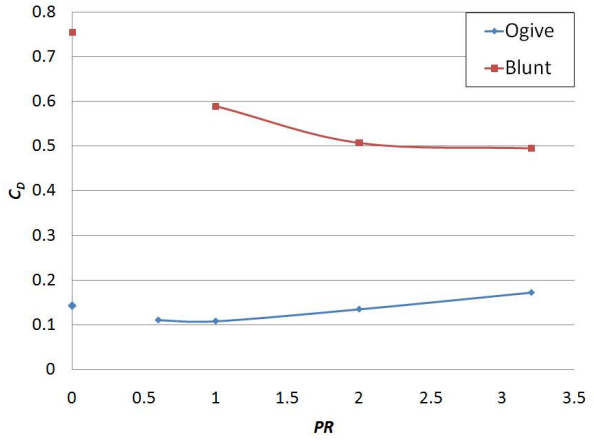

Fig.13. Comparison of the drag coefficients of the ogive body and blunt body

4 Extended Nozzle Model

From the section 3, it was found that it is really important to avoid constructing the recompressed shock for this thermal protection system by using the opposing jet. In addition, smaller mass flow rate is desirable in practical sense. Therefore, it is required to find out more

efficient ways as for this thermal protection system other than increasing total pressure ratio.

In this section the ogive body with extended nozzle is proposed as one of the possible improved examples. The configuration of this extended nozzle model is shown in Fig.14 as the grid figure around the nose tip. In this figure, the original ogive configuration is also shown to understand the difference between the models.

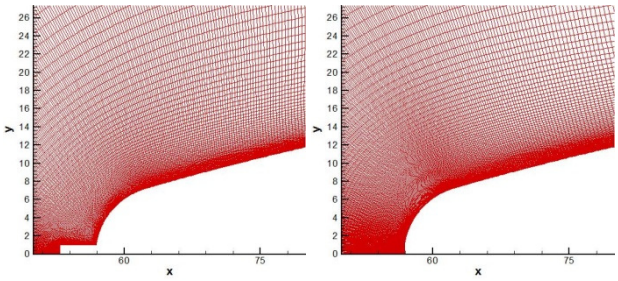

Fig.14. Comparison of the configurations of the models with and without extended nozzle.

The flow field has been simulated under the conditions shown in Table.3. Other conditions are the same as shown in Table.2.

Table.3. Flow conditions for extended nozzle model

<Opposing Jet>		
Total pressure ratio	PR	0.6
<Nozzle>		
Nozzle length	L_n[mm]	3.0, 4.0, 5.0

Since $PR = 0.6$ is the case which is bothered by high maximum heat flux due to strong recompressed shock, we will apply the extended nozzle model only to this case to investigate the effectiveness of this model.

The results of these three cases are shown in Fig.15 with the result of $PR = 0.6, 2.0$ cases without extended nozzle. From this figure, it can be seen that all three cases could reduce aerodynamic heating compared with the case of $PR = 0.6$ without extended nozzle. In addition to that, the heat flux values are almost as same as that of $PR = 2.0$ case. Among those three cases, the case of $L_n = 4.0$ mm could achieve the most significant heat flux reduction, which is 80% reduction of maximum heat flux value from the case of $PR = 0.6$ without extended nozzle. This huge aerodynamic heat reduction is achieved by weakening recompressed shock. From Fig.16, it can be seen that there remains slight recompressed shock in the case of $L_n = 4.0$ mm, while strong recompressed shock can be seen in the case without extended nozzle. Besides, it is found that there is an optimal nozzle length for the specified freestream Mach number and PR.

As discussed above, this model proposed here succeeded to reduce aerodynamic heat without increasing mass flow rate of the opposing jet. This result is desirable for the bodies which has some constrains in terms of total mass and space, such as RLV.

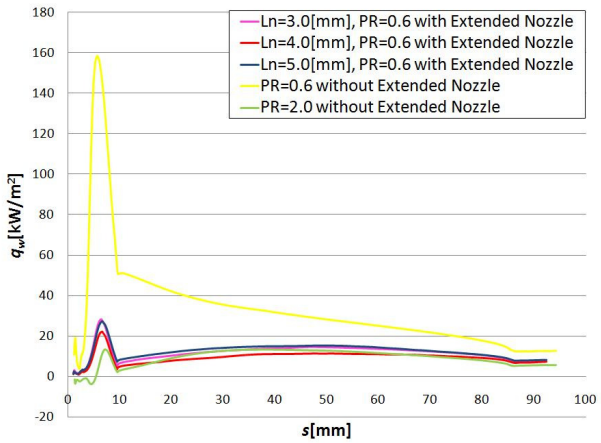

Fig.15. Heat flux distribution for extended nozzle model and $PR = 0.6, 2.0$ without extended nozzle

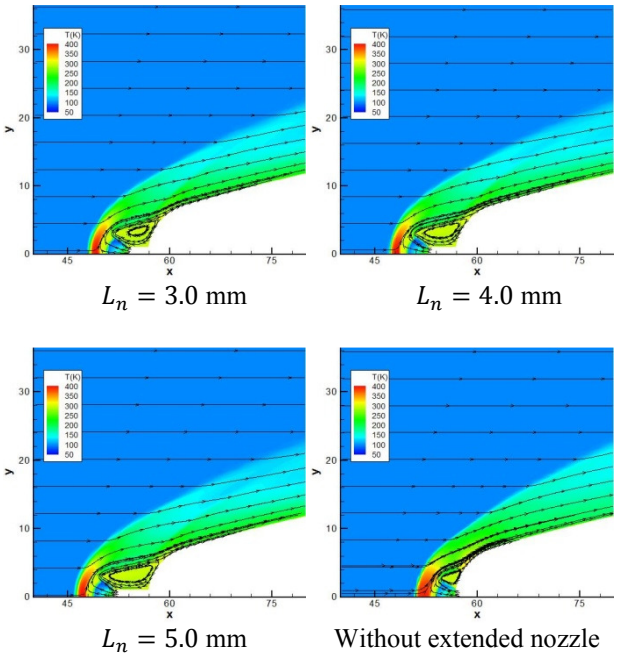

Fig.16. Temperature contour and streamline of the model with and without extended nozzle in the case of $PR = 0.6$

5 Conclusions

The conclusions of this study are the followings.

1) The opposing jet can also reduce aerodynamic heating for the ogive body whose drag is smaller than that of the blunt body.

2) The effect of the opposing jet on reduction of aerodynamic heating varies significantly by the nose configuration even with constant mass flow rate.

3) It is proved to be essential to avoid constructing the recompressed shock right in front of the surface of nose region in order to reduce the aerodynamic heating around the nose region by the opposing jet.

References

[1] K. Hayashi, S. Aso, and Y. Tani**.** Numerical Study of Thermal Protection System by Opposing Jet. *AIAA-paper*, No. AIAA-2005-188, 2005.

[2] K. Hayashi, S. Aso, and Y. Tani. Experimental Study of Thermal Protection System by Opposing Jet in Supersonic Flow. *Journal of Spacecraft and Rockets,* Vol. 43, No. 1, pp. 233-238, 2006

[3] G. Cheng, K. Neroorkar, Y. Chen, T. Wang and E. Daso. Numerical Study of Flow Augmented Thermal Management for Entry and Re-entry Environments. *25th AIAA Applied Aerodynamics Conference, Miami*, FL, June 25-28, 2007.

[4] Afsheen Khamooshi, Trent Taylor and David W. Riggins. Drag and Heat Transfer Reductions in High-Speed Flows. *AIAA Journal*, Vol. 45, No. 10, October 2007.

[5] Wada Y. and Liou M.S., A flux splitting scheme with high-resolution and robustness for discontinuities. *AIAA-paper*, No. AIAA-94-0083, 1992.

[6] J. E. Bardina, P. G. Huang and T. J. Coakley. Turbulence Modeling Validation, Testing, and Development. *NASA Technical Memorandum 110446*, 1997.

[7] Wilcox DC. Formulation of the $k-\omega$ Turbulence Model Revisited. *45th AIAA Aerospace Sciences Meeting and Exhibit*, Jan 2007.

[8] Craft T.J, Launder B.E, and Suga K. Development and application of a cubic eddy-viscosity model of turbulence. *International Journal of Heat and Fluid Flow*, Vol. 17, pp. 108-115, 1996.

[9] Fay J.A. and Riddell F.R., Theory of stagnation point heat transfer in dissociated air. *Journal of the Aeronautical Sciences*, Vol. 25, No. 2, pp. 73-85, 1958.

[10] Finley P.J. The flow of a jet from a body opposing a supersonic free stream., *J. Fluid Mech.*, Vol. 26, No. 2, pp. 337-368, 1966.

[11] Obayashi S., Matsushima K., Fujii K., and Kuwahara K., Improvements in efficiency and reliability for navier-stokes computations using the lu-adi factorization algorithm. *AIAA-paper*, No. AIAA-86-0338, 1986.

Copyright Statement